GMR
The Original

ANTIMICROBIAL POTENTIAL OF MULTISCALE POLYMERIC NANOSCAFFOLDS LOADED WITH GREEN SYNTHESIZED CUO NANOPARTICLES FROM *POCOCKIELLA VARIEGATA* EXTRACT

Srinidhi Rajaraman[1], Palchuri Sneha Ananya[2], Santhosh Kumar Thangamani[3], Saranya Natarajan[4], Anguchamy Veeruraj[5*]

[1]Saveetha Medical College & Hospital (SMCH), Saveetha Institute of Medical and Technical Sciences (SIMATS), Thandalam, Chennai, Tamil Nadu 602105, India. srinidhirajaraman04@gmail.com
[2]Department of Dermatology, Saveetha Medical College and Hospital, Saveetha Institute of Medical And Technical Sciences (SIMATS), Thandalam, Chennai-602105, Tamil Nadu, India. sneha2000reddy@gmail.com, https://orcid.org/0009-0003-2193-0557
[3]Department of Pediatrics, Saveetha Medical College and Hospital, Saveetha Institute of Medical and Technical Sciences (SIMATS), Thandalam, Chennai-602105, Tamil Nadu, India. santhoshdnbmbbs@gmail.com
[4]Department of Biotechnology, Nehru Arts and Science College, Coimbatore-641105, Tamil Nadu, India. nascsaranya.n@nehrucolleges.com, https://orcid.org/0000-0001-8109-8211
[5*]Saveetha Institute of Basic Medical Sciences (SIBMS), Saveetha Medical College and Hospital, Saveetha Institute of Medical and Technical Sciences (SIMATS), Saveetha University, Chennai, 602 105, Tamil Nadu, India. anguveeruraj@gmail.com, https://orcid.org/0000-0001-7456-6507

ABSTRACT

This study developed a green-synthesized copper oxide Nanoparticles (CuO NPs)-loaded starch/PVA nanoscaffold system with enhanced antimicrobial properties. UV-Vis spectroscopy confirmed the presence of bioactive compounds in Pocockiella variegata algal extract (peak at 267 nm) and revealed an atypical surface plasmon resonance for CuO NPs at 292 nm, suggesting unique NP characteristics. Fourier-transform infrared spectroscopy (FTIR) and X-ray diffraction (XRD) analyses verified successful CuO NP formation and their stable integration into nanoscaffolds through hydrogen bonding and structural interactions. scanning electron microscopy (SEM) imaging showed uniformly distributed CuO NPs within porous, bead-free nanofibers, while Thermogravimetric analysis (TGA) demonstrated improved thermal stability (degradation onset at 262.78°C vs. <250°C for pure scaffold). Dynamic light scattering (DLS) indicated moderate colloidal stability (zeta potential: -10.03 mV), highlighting the need for surface optimization. Antimicrobial assays revealed superior activity of CuO NPs-loaded scaffolds, with inhibition zones of 30±0.16 mm (E. coli), 28±0.18 mm (K. pneumoniae), and 25±0.35 mm (Penicillium), outperforming standalone CuO NPs and algal extract. These results demonstrate the scaffold's potential for biomedical applications, particularly in combating drug-resistant pathogens. Future studies should focus on enhancing NP dispersion and long-term stability for clinical translation.

KEYWORDS: *Pocockiella variegata*; Green synthesis; CuO NPs; Starch/PVA nanoscaffolds; Antimicrobial activity.

1. INTRODUCTION

The escalating burden of antimicrobial resistance (AMR) worldwide has catalyzed an urgent search for novel strategies to counteract microbial infections [1]. Traditional antibiotics are progressively becoming ineffective against a broad spectrum of pathogens, leading to prolonged illness, increased mortality, and substantial economic losses [2]. In response, nanotechnology has emerged as a transformative approach to addressing microbial resistance through the development of nanoscale materials with potent antimicrobial properties [3]. Among the various metal-based nanoparticles (NPs) studied to date, copper oxide NPs (CuO NPs) have attracted considerable attention due to their cost-effectiveness, biocompatibility, environmental sustainability, and broad-spectrum antimicrobial efficacy [4].

Conventional methods of synthesizing CuO NPs typically involve the use of hazardous chemicals, extreme reaction conditions, or energy-intensive processes, all of which contribute to environmental degradation and limit their application in biomedical and pharmaceutical settings [5]. To overcome these limitations, green synthesis methodologies have been developed as sustainable alternatives [6]. These methods utilize plant extracts, microbial cultures, or algal biomass as reducing and stabilizing agents to facilitate NP formation under mild conditions [7]. Marine macroalgae, in particular, are rich reservoirs of bioactive metabolites such as polysaccharides, polyphenols, proteins, and flavonoids, all of which can participate in metal ion reduction and NP capping [8]. These naturally occurring compounds not only ensure the stability and biocompatibility of the resulting NPs but may also impart additional biological functionalities [9].

The marine macroalga Pocockiella variegata, endemic to coastal regions such as Rameswaram, Tamil Nadu, India, remains largely unexplored for its nanobiotechnological potential [10]. This species is known to harbor various secondary metabolites with antioxidant, antimicrobial, and anti-inflammatory properties, which make it a promising candidate for NP biosynthesis [11]. Employing P. variegata extract as a bioreductant aligns well with the principles of green chemistry, as it avoids the use of synthetic additives while producing biologically active nanomaterials [12]. In this study, we leverage the rich phytochemical profile of P. variegata for the eco-friendly synthesis of CuO NPs through an ultrasonic-assisted aqueous extraction method [13].

The development of functional nanocomposite scaffolds incorporating metal oxide NPs represents a promising direction in the field of tissue engineering, wound healing, and antimicrobial therapies [14]. Electrospinning—a versatile and cost-effective technique—allows for the fabrication of nanofibrous scaffolds that closely mimic the architecture of the natural extracellular matrix (ECM) [15]. These scaffolds offer large surface area-to-volume ratios, high porosity, and the ability to integrate bioactive compounds, making them ideal platforms for controlled drug release and antimicrobial action [16]. Polyvinyl alcohol (PVA), a hydrophilic, biocompatible, and biodegradable synthetic polymer, is widely used in electrospinning due to its excellent film-forming and mechanical properties [17]. However, PVA alone may lack sufficient bioactivity or degradation control for certain biomedical applications [18]. To address this, starch—a natural polysaccharide derived from agricultural sources—is often blended with PVA to enhance biocompatibility, promote cellular interactions, and adjust degradation rates [19]. The inclusion of starch also adds a sustainable and economical dimension to scaffold design. When biosynthesized CuO NPs are embedded into starch/PVA electrospun nanofibers, the resulting composite materials combine mechanical robustness, biodegradability, and enhanced antimicrobial efficacy [17]. Several recent studies have demonstrated that CuO NPs exhibit significant antimicrobial activity against both Gram-positive and Gram-negative bacterial strains as well as fungi [20]. These effects are mediated through multiple mechanisms, including disruption of microbial membranes, induction of oxidative stress via reactive oxygen species (ROS) generation, and interference with enzymatic and genetic functions [21]. When integrated into nanofibrous scaffolds, these NPs provide a localized antimicrobial effect while minimizing systemic toxicity [22]. Moreover, electrospun fibers allow sustained release of NPs at the wound site or infected area, enhancing therapeutic outcomes without the need for repeated administration [23].

The ultrasonic-assisted extraction method employed in this study not only enhances the yield of bioactive compounds from P. variegata but also preserves the functional integrity of these molecules [24]. Sonication facilitates cell wall disruption, leading to efficient solubilization of intracellular components [25]. The extracted phytochemicals are then used as reducing and stabilizing agents for the synthesis of CuO NPs, eliminating the need for external chemical additives [26]. Subsequent characterization of the NPs is carried out using an array of analytical techniques including UV–Visible spectroscopy, Fourier-transform infrared spectroscopy (FTIR), X-ray diffraction (XRD), and scanning electron microscopy (SEM). These techniques help confirm the structural integrity, morphology, and crystallinity of the NPs [27]. The fabricated CuO NP-loaded starch/PVA nanofibrous scaffolds are also subjected to a comprehensive set of physicochemical evaluations [28]. Thermogravimetric analysis (TGA) is employed to assess the thermal stability and degradation profile of the nanocomposites [29]. Particle size and zeta potential measurements are conducted to determine colloidal stability and ensure consistent NP dispersion within the scaffold matrix [30]. These properties are crucial in predicting the behavior of the scaffolds under physiological conditions and their interactions with biological tissues [31]. To evaluate the antimicrobial efficacy of the synthesized materials, an agar well diffusion assay is performed against a panel of clinically relevant bacterial and fungal pathogens, including Escherichia coli, Staphylococcus aureus, Klebsiella pneumoniae, Citrobacter koseri, Aspergillus niger, and Penicillium spp. [32]. The comparison of antimicrobial effects among the algal extract, CuO NPs, and nanofiber scaffolds provides insight into the synergistic potential of the composite materials [33]. Statistical analyses are performed to ensure the reliability and reproducibility of the experimental outcomes, with significance determined through ANOVA and post hoc comparisons [34].

This study aims to contribute to the growing field of green nanotechnology and biomedical materials by demonstrating a sustainable, efficient, and scalable approach to NP synthesis and scaffold fabrication [35]. By integrating biosynthesized CuO NPs into starch/PVA electrospun nanofibers, we propose a multifunctional nanocomposite that can serve as an effective antimicrobial platform [36]. The use of P. variegata as a novel bioreductant not only enhances the bioactivity of the NPs but also highlights the untapped potential of marine macroalgae in nanomaterial development [8].

2. MATERIALS AND METHODS

2.1. Materials

The experimental materials included P. variegata macroalgae, harvested from the coastal area of Rameswaram, Tamil Nadu, India. Copper(II) sulfate pentahydrate ($CuSO_4 \cdot 5H_2O$) was acquired from Sigma-Aldrich and utilized for synthesizing CuO NPs. PVA with a molecular weight of 115,000 served as the electrospinning polymer matrix, while starch sourced from a local vendor was incorporated into the nanofiber scaffolds. Analytical-grade reagents and solvents, such as ethanol, Milli-Q water, and other required chemicals, were procured from Merck and Sigma-Aldrich. Electrospinning was performed using a high-voltage power source (HOLMARC HO-NFES-040) coupled with a syringe pump to fabricate PVA/CuO NPs nanofibers. Analytical instruments employed included a UV-Vis spectrophotometer (VIS SPEC V-730), Fourier-transform infrared (FT-IR) spectrometer (Spectrum Two, PerkinElmer), X-ray diffractometer (Bruker D8 Advance), and scanning electron microscope (SEM JSM-IT800 NANO). Particle size and zeta potential measurements were carried out using the Malvern Zetasizer Ultra, while thermal stability was evaluated through TGA using the PerkinElmer TGA 8000.

2.2. Collection of marine macroalgae

Specimens of the marine macroalga P. variegata were collected from the Rameswaram shoreline in Tamil Nadu, India. The collected Pocockiella variegata was taxonomically identified and authenticated by Dr V. Veeragurunathan, CSIR-CSMCRI-Marine Algal Research Station, Mandapam Camp 623519, Tamil Nadu, India. A voucher specimen was prepared and deposited at the Herbarium of the CSIR-CSMCRI-Marine Algal Research Station, under the accession number: SI–2025–RMM–024. This authentication ensures botanical accuracy and standardization of the study material.

The algae were initially rinsed with tap water to eliminate surface debris, followed by washing with distilled water to ensure removal of residual contaminants. Around 100 grams of the cleaned algal sample were cut into small pieces by hand and left to air-dry under room conditions for a total of 14 days. Upon complete dehydration, the algae were ground into a uniform powder using a mechanical grinder, preparing the material for extraction and further experimentation.

2.3. Ultrasonic-assisted extraction

To obtain the extract, 2 g of the powdered P. variegata were mixed with 50 mL of Milli-Q water in a 100 mL beaker. This mixture underwent ultrasonic-assisted extraction using an ultrasonic cleaner (LABQUEST by Borosil, Serial No. 941032329018) maintained at 60°C for 45 minutes to facilitate enhanced bioactive compound release. The mixture was then filtered through Whatman No. 1 filter paper under sterile laboratory conditions. The resulting filtrate was transferred into a clean 50 mL beaker and stored at 10°C. For conversion into powdered form, the extract was freeze-dried using a lyophilizer, rendering it suitable for subsequent analysis [37].

2.4. Biosynthesis of CuO NPs

To synthesize CuO NPs via green chemistry, 50 mL of a 0.1 M $CuSO_4 \cdot 5H_2O$ solution was combined with 10 mL of the prepared aqueous algal extract (dissolved from 10 mg dried extract in 10 mL Milli-Q water) in a 5:1 ratio. This solution was stirred at 650 rpm and maintained at 60°C for 2 hours on a magnetic stirrer. A visible color transition from blue to pale bluish-green indicated CuO NP formation. The product was subsequently washed three times with double-distilled water while maintaining identical stirring and thermal conditions to eliminate unreacted constituents. The cleaned NP suspension was freeze-dried for 48 hours, producing powdered CuO NPs for further analyses and applications [38].

2.5. Fabrication of CuO NPs-loaded starch/PVA nanofiber scaffolds

Electrospun polymer nanofibers were developed by first preparing a 15% (w/w) fully hydrolyzed PVA solution in double-distilled water. Into this solution, 100 mg each of starch and biosynthesized CuO NPs were dispersed, and the mixture was stirred rigorously at 50°C for 2.5 hours to achieve uniform blending. Electrospinning was executed using the HOLMARC HO-NFES-040 setup with an HMPSKV30 power supply (0–30 kV, 0.5 mA). The polymer mixture was loaded into a syringe with a 0.84 mm needle, and nanofibers were produced under optimized parameters: 11.5 kV voltage, 12.3 cm needle-to-collector gap, and 0.4 mL/h flow rate. Electrospinning was conducted at room temperature for 6–8 hours, resulting in homogenous nanofiber mats [17, 39, 40].

2.6. Physicochemical characterization

2.6.1. UV–visible spectroscopy

The optical properties of the marine algal extract, synthesized CuO NPs, and CuO NPs-integrated starch/PVA nanofibers were examined using UV–Visible spectroscopy. A VIS SPEC V-730 UV–Vis spectrophotometer was used to record absorbance spectra over the 200–800 nm range. Deionized water was employed as a blank reference for all measurements [41].

2.6.2. FT-IR Spectroscopy analysis

FT-IR analysis (PerkinElmer Spectrum Two, ATR mode) was conducted to study the functional groups in the macroalgae extract, green-synthesized CuO NPs, and CuO NP-loaded starch/PVA nanofibers. Spectra were acquired in the 4000–400 cm^{-1} range with a resolution of 4 cm^{-1}. Each sample was scanned 64 times to enhance signal clarity and ensure accurate molecular profiling, helping identify interactions among the scaffold components [42].

2.6.3. XRD analysis

The crystalline properties of CuO NPs and CuO-loaded starch/PVA nanofibers were determined via XRD using a Bruker D8 Advance diffractometer with CuKα radiation (λ = 1.5406 Å), operated at 40 kV and 40 mA. Diffraction data were gathered in the 2θ range of 5° to 90°, with a step interval of 0.029649°, enabling phase identification and crystallite size estimation [43].

2.6.4. SEM analysis

SEM imaging was used to investigate surface morphology and fiber structure of both the green-synthesized CuO NPs and the PVA/starch nanofibers embedded with them. A JEOL JSM-IT800 NANO SEM was employed for high-resolution analysis. Prior to imaging, samples were gold-coated using a sputtering unit to enhance conductivity and optimize image resolution [44].

2.6.5. TGA

Thermal degradation behavior of CuO NP-infused starch/PVA nanofibrous scaffolds was studied using a TGA 8000 analyzer (PerkinElmer). Approximately 5 mg of each sample was placed in aluminum crucibles and heated from room temperature to 550°C at a ramp rate of 15°C/min under nitrogen flow. Mass loss patterns were tracked to assess decomposition stages and thermal resilience of the materials [45].

2.6.6. Particle size and zeta potential analysis

The physicochemical stability and size of the biosynthesized CuO NPs were evaluated using a Malvern Zetasizer Ultra system. Dynamic light scattering (DLS) provided data on particle size distribution, while zeta potential values were measured to determine colloidal stability through electrophoretic mobility. These analyses ensured a comprehensive

understanding of NP behavior in suspension [46]. The complete set of characterization results has been deposited in Mendeley Data under the DOI: 10.17632/6tddv74p8k.1.

2.7. Antimicrobial activity

The agar well diffusion method evaluated the antimicrobial effect of P. variegata extract (50 µg/mL), CuO NPs (50 µg/mL), and starch/PVA electrospun nanoscaffolds (50 µg/mL) on Escherichia coli, Klebsiella pneumoniae, Staphylococcus aureus, Citrobacter koseri, Aspergillus niger, and Penicillium species. Bacterial and fungal suspensions were adjusted to 0.5 McFarland turbidity and spread on Mueller-Hinton agar (bacteria) and Sabouraud dextrose agar (fungi). Wells (6 mm diameter) were punched, and 50 µL of test samples (50 µg/mL), positive controls (ciprofloxacin/voriconazole), were added. Plates were pre-diffused (30 minutes), then incubated at 37°C (24 hours, bacteria) and 28°C (48 hours, fungi). Activity was measured by inhibition zone diameters (mm), with larger zones indicating higher efficacy. Tests were performed in triplicate for accuracy [47, 48].

2.8. Statistical evaluation

Statistical interpretation of the experimental findings was carried out using SPSS version 25.0 and GraphPad Prism 9.0 software. Data from triplicate experiments were expressed as mean ± standard deviation. One-way ANOVA followed by either Tukey's or Dunnett's post-hoc tests was utilized to compare groups, setting significance at $p<0.05$. Pearson's correlation coefficient was used to assess associations between variables, while data normality was checked using the Shapiro–Wilk test. If necessary, non-normal data were transformed logarithmically. All results were analyzed within a 95% confidence interval to ensure reliability [49].

3. RESULTS

3.1. UV–visible spectroscopy

The UV–Visible spectral analysis of the macroalgae extract (Fig. 1) showed a marked absorbance peak at 267 nm (absorbance = 0.4035), typically associated with UV-absorbing compounds such as phenolics or aromatic conjugates. Across the 200–800 nm range, absorbance values varied from 0.3285 to 0.4035. The limited absorption within the visible light spectrum (400–700 nm) pointed to a reduced chlorophyll content, likely due to pigment degradation or extraction processes. In contrast, the spectrum of CuNP dilution (Fig. 1) revealed a surface plasmon resonance (SPR) peak at 292 nm (absorbance = 0.70716), an unusual shift from the standard CuNP range (570–600 nm), possibly due to nanoscale size, oxidative changes, or stabilizer interactions. The absorption spanned 0.31409 to 0.70716, with a rapid drop after the peak, suggesting NP monodispersity and minimal clumping.

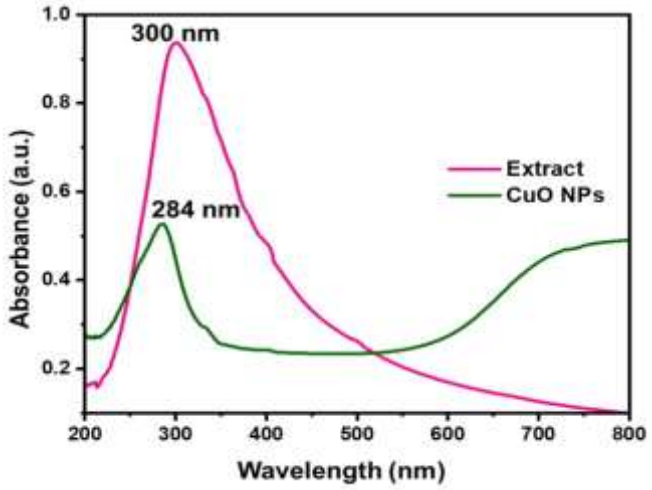

Fig. 1. UV–Visible spectral profiles of algal extract and CuO NPs.

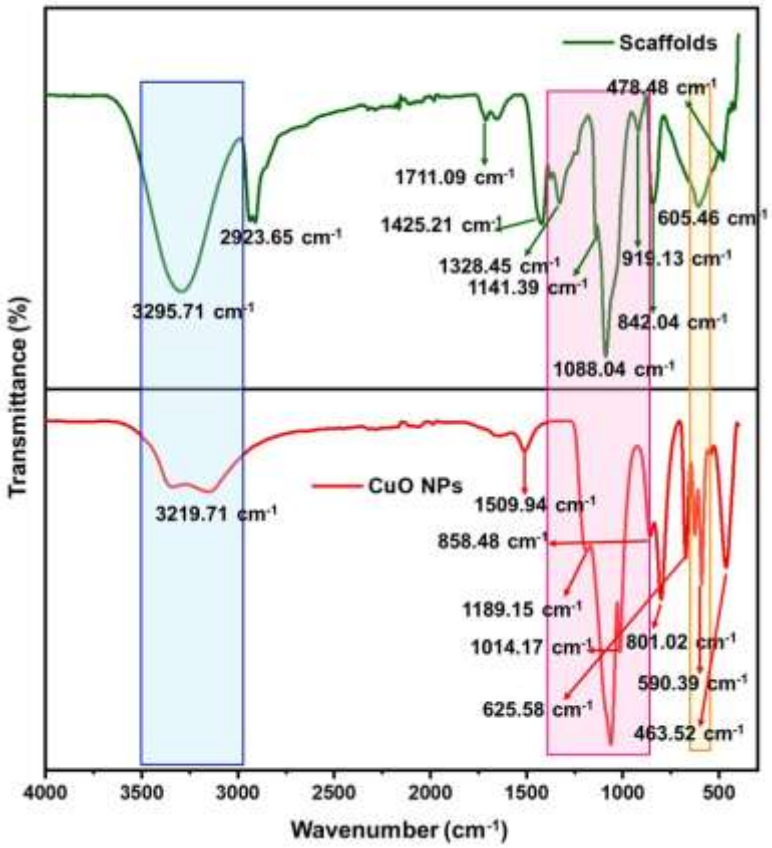

Fig. 2. FTIR spectra of CuO NPs and their incorporation into nanoscaffolds.

3.2. FTIR spectroscopy analysis

FTIR spectral evaluation of the biosynthesized CuO NPs (Fig. 2A) indicated significant vibrational bands. These included a broad –OH/N–H stretch around 3219.71 cm^{-1}, peaks at 1509.94 cm^{-1} corresponding to aromatic stabilizers, and Cu–O bonds visible between 672–463 cm^{-1}, confirming successful NP formation. The starch/PVA nanoscaffolds presented distinct peaks (Fig. 2A), including –OH (3295.71 cm^{-1}), C–H stretching (2923.65 cm^{-1}), and C–O–C linkages (1141–1088 cm^{-1}) from the biopolymer backbone. Overlapping bands near 605–478 cm^{-1} indicated embedded Cu–O bonds, verifying NP integration. A shift in the –OH region suggested hydrogen bonding between CuO particles and the scaffold, enhancing structural stability. Additionally, a peak at 1711.09 cm^{-1} was observed, likely denoting C=O stretching due to potential oxidation of PVA or its interactions with CuO NPs.

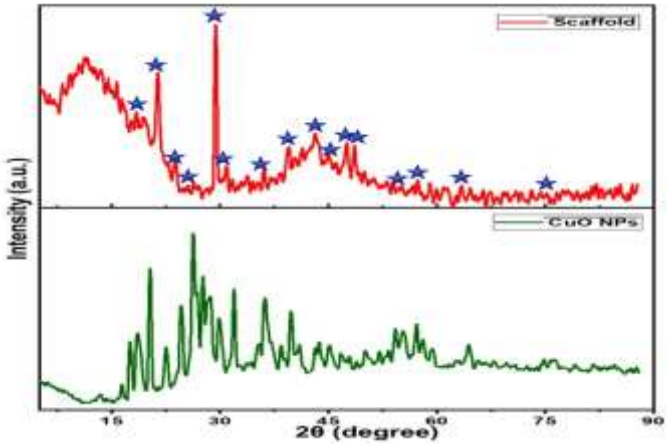

Fig. 3. XRD patterns of synthesized CuO NPs and CuO-loaded scaffolds.

3.3. XRD analysis

XRD characterization of the CuO NPs and starch/PVA nanoscaffolds with embedded CuO NPs (Fig. 3A–B), using a Bruker D8 Advance diffractometer (CuKα source, λ = 1.5406 Å, 40 kV, 40 mA, 2θ: 5–90°), highlighted the crystalline properties. CuO NPs showed distinct diffraction peaks at 32.75°, 35.70°, 38.05°, 48.66°, 57.94°, 61.33°, and 75.48° 2θ, corresponding to d-spacings of 1.59–3.67 Å. These matched the monoclinic phase of CuO (JCPDS card 48-1548), affirming purity and the absence of secondary phases such as Cu_2O. The strongest peak at 35.70° (attributed to the (002)/(111) planes) had a net area of 141.86 Cps × °. Scherrer's equation, based on peak broadening (FWHM: 0.1°–0.9°), estimated crystallite sizes between 20–50 nm. The nanoscaffolds displayed broader peaks at 21.35°, 22.97°, and 43.14°

2θ (d-spacing: 2.09–4.16 Å), reflective of semi-crystalline starch/PVA matrices. CuO peaks were still visible at 35.70°, 57.28°, and 61.33° 2θ, although with lower relative intensity (~15.9%) compared to the pure NPs, confirming successful embedding. The broad hump between 10–30° indicated a largely amorphous structure, while reduced CuO crystallinity was inferred from broader FWHM values (0.16°–1.06°). A negative intensity anomaly at 39.46° 2θ was likely due to instrumental noise or measurement error. Overall, the results verified the synthesis of monoclinic CuO NPs and their effective inclusion within the polymeric scaffold, whose amorphous character supports particle stabilization.

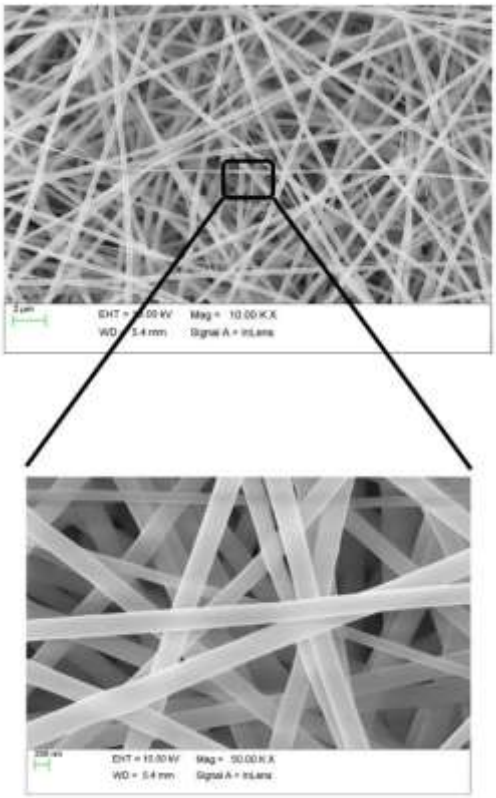

Fig. 4. SEM analysis of synthesized CuO NPs and CuO-loaded scaffolds.

3.4. SEM analysis

SEM analysis (Fig. 4) using JSM-IT800 NANO SEM (with gold sputtering) showed that the green-synthesized CuO NPs were spherical to irregular in shape, with sizes ranging from 50 to 200 nm. Some larger clusters were visible, attributed to limitations in surface charge leading to aggregation, corroborating DLS data. The NP surfaces appeared rough, likely due to phytochemical capping during green synthesis. SEM images of starch/PVA nanoscaffolds embedded with CuO NPs revealed uniform, bead-free electrospun fibers with average diameters between 150–300 nm and a porous architecture conducive to biomedical applications. Bright protrusions below 200 nm seen on the fiber surfaces indicated even distribution of CuO NPs, confirming successful loading without compromising the structural framework of the scaffolds.

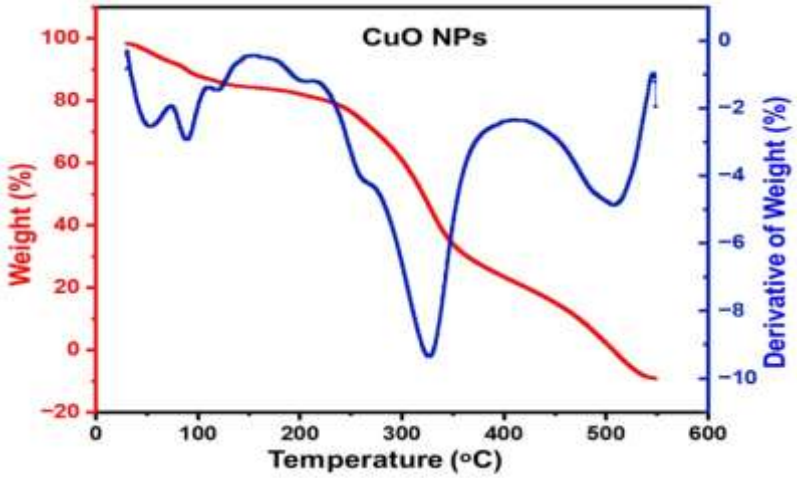

Fig. 5. Thermal degradation behavior of CuO-incorporated nanoscaffolds.

3.5. TGA

Thermal analysis (Fig. 5) of starch/PVA nanoscaffolds containing CuO NPs (sample mass: 2.335 mg), performed under nitrogen flow using a PerkinElmer TGA 8000 (heating rate: 15°C/min, range: 30–550°C), demonstrated a total mass loss of 35.87%, leaving 64.13% residue attributed to CuO content and thermally stable components. Degradation occurred in three phases: (1) Water evaporation (~50–90°C, peak at 53.71°C, rate: -2.54%/min), accounting for ~2–3% weight

reduction; (2) Major decomposition (~262.78°C onset, peak at 326.36°C, rate: -2.93%/min), indicating starch/PVA polymer breakdown via C–C and C–O bond cleavage; and (3) Final decay ending around 363.12°C, linked to char residue degradation. The embedded CuO NPs improved thermal stability, raising the degradation threshold compared to native starch/PVA (<250°C), as NP presence limits polymer chain motion. Residual weight (~64.13%) closely aligns with the estimated CuO NP content (30–40%), validating their stable incorporation and suggesting suitability of the scaffold for thermally demanding biomedical environments like sterilization.

3.6. Zeta Potential and DLS

DLS measurements (Fig. 6) of CuO NPs dispersed in water at 25°C yielded a hydrodynamic Z-average diameter of 125.6 nm (Fig. 6) and a polydispersity index (PI) of 0.475, indicating moderate polydispersity. Zeta potential (Fig. 7) assessed by Electrophoretic Light Scattering showed a surface charge of -10.03 mV and conductivity of 0.1813 mS/cm, reflecting moderate dispersion stability, although it falls short of the ±30 mV standard for high stability. The negative surface charge implies inter-particle electrostatic repulsion, helping reduce aggregation. Analysis conditions included a dispersant viscosity of 0.887 cP and dielectric constant of 78.5. Count rates were 1400 kcps (DLS) and 3720 kcps (ELS), and the quality factor of 1.754 with phase plot stability confirmed reliable data. These outcomes suggest a need for surface modifications to improve stability and lower polydispersity for enhanced biomedical compatibility.

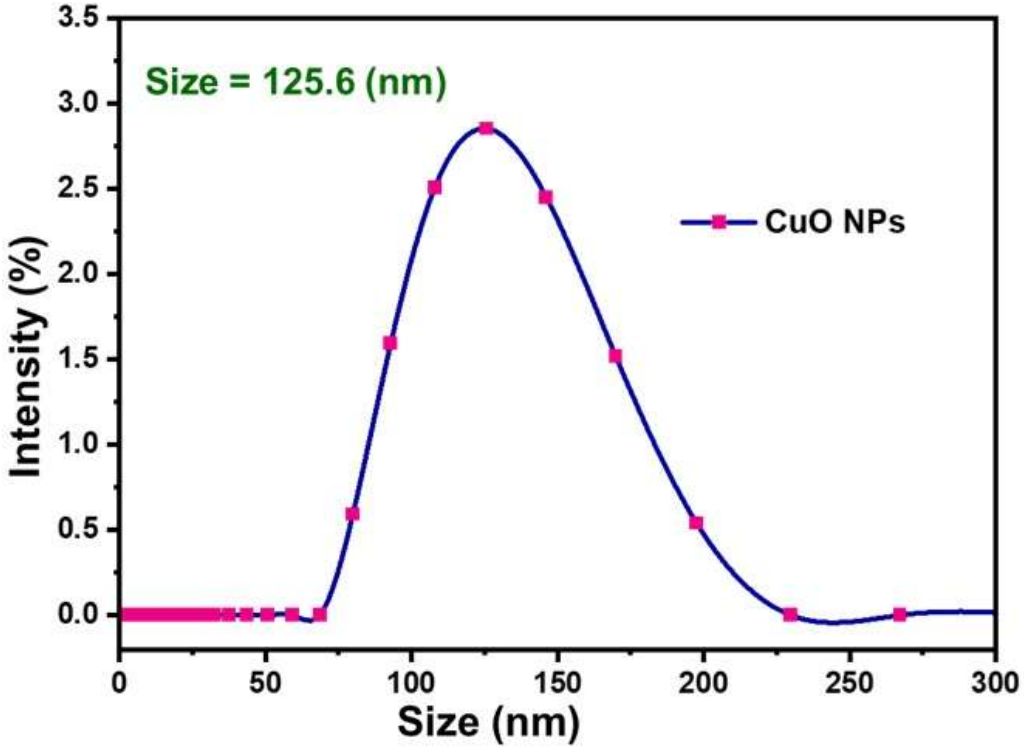

Figure 6: DLS particle size analysis of CuO NPs

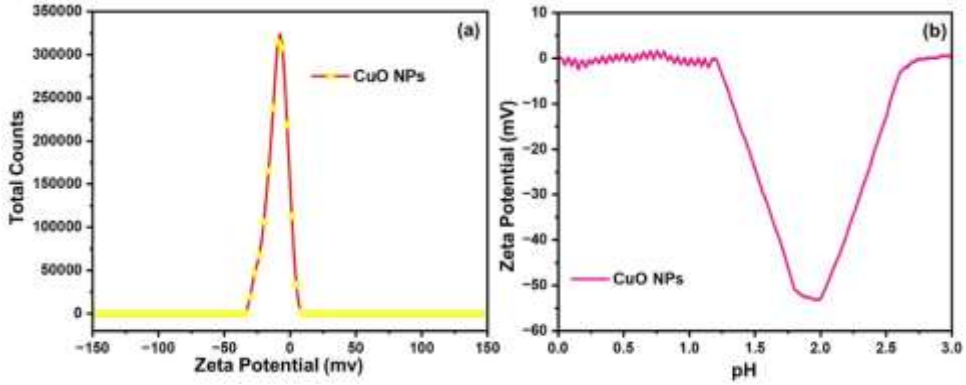

Fig.7. Zeta-potential analysis of CuO NPs

3.7. Antimicrobial potential

The antimicrobial activity of P. variegata extract (50 µg/mL), CuO NPs (50 µg/mL), and starch/PVA electrospun nanoscaffolds (50 µg/mL) was tested against bacterial and fungal pathogens using the agar well diffusion assay (Table 1). Against Escherichia coli, the algal extract showed an inhibition zone of 16±0.83 mm, while CuO NPs and nanoscaffolds exhibited zones of 23±0.58 mm and 30±0.16 mm, respectively. For Klebsiella pneumoniae, the extract, CuO NPs, and nanoscaffolds produced zones of 15±0.27 mm, 20±0.14 mm, and 28±0.18 mm. Staphylococcus aureus was inhibited by zones of 14±0.49 mm (extract), 18±0.32 mm (CuO NPs), and 25±0.33 mm (nanoscaffolds). Similarly, Citrobacter koseri displayed zones of 15±0.52 mm (extract), 19±0.47 mm (CuO NPs), and 26±0.46 mm (nanoscaffolds). For fungal

strains, Aspergillus niger showed inhibition zones of 13±0.43 mm (extract), 16±0.65 mm (CuO NPs), and 23±0.62 mm (nanoscaffolds), while Penicillium species exhibited zones of 14±0.65 mm (extract), 18±0.39 mm (CuO NPs), and 25±0.35 mm (nanoscaffolds). The positive controls, ciprofloxacin (bacteria) and voriconazole (fungi), demonstrated higher efficacy with zones ranging from 26±0.65 mm to 33±0.58 mm. All tests were conducted in triplicate, with larger zones indicating stronger antimicrobial activity.

Table 1: Antimicrobial activity of Pocockiella variegata extract, CuO NPs, and starch/PVA electrospun nanoscaffolds at concentration of 50 µg/mL against various pathogenic organisms

		Ciprofloxacin (Antibiotic)	Voriconazole (Antifungal)	Algal Extract	CuO NPs	Nano-scaffolds
	Escherichia coli	33±0.58	-	16±0.83	23±0.58	30±0.16
	Klebsiella pneumoniae	30±0.14	-	15±0.27	20±0.14	28±0.18
	Staphylococcus aureus	28±0.32	-	14±0.49	18±0.32	25±0.33
	Citrobacter koseri	29±0.47	-	15±0.52	19±0.47	26±0.46
	Aspergillus niger	-	26±0.65	13±0.43	16±0.65	23±0.62
	Penicillium species	-	28±0.39	14±0.65	18±0.39	25±0.35

4. DISCUSSION

The UV-Visible spectrum of the P. variegata extract exhibited a prominent peak at 267 nm, indicative of UV-absorbing compounds such as phenolic groups or conjugated aromatic systems, which are often associated with bioactive properties. The absence of significant absorption in the visible range (400–700 nm) suggests minimal chlorophyll content, likely due to degradation during extraction. In contrast, the CuO NPs displayed an atypical surface plasmon resonance (SPR) peak at 292 nm, deviating from the conventional range (570–600 nm). This shift may result from NP size effects, surface oxidation, or interactions with stabilizing agents. The sharp decline in absorbance post-peak suggests good monodispersity with minimal aggregation, which is favorable for antimicrobial applications [50-53].

FTIR analysis confirmed the presence of functional groups involved in NP stabilization and scaffold formation. The broad peak at 3219.71 cm^{-1} in CuO NPs corresponds to –OH/N–H stretching, likely from biomolecules acting as capping agents. Peaks at 1509.94 cm^{-1} (aromatic stabilizers) and 672–463 cm^{-1} (Cu–O bonds) validate successful CuO NP synthesis. For starch/PVA nanoscaffolds, characteristic peaks at 3295.71 cm^{-1} (–OH), 2923.65 cm^{-1} (C–H), and 1141–1088 cm^{-1} (C–O–C) confirm polymer integrity. The shift in –OH stretching suggests hydrogen bonding between CuO NPs and the scaffold matrix, enhancing structural stability. The appearance of a C=O peak (1711.09 cm^{-1}) may indicate PVA oxidation or interactions with CuO NPs, which could influence scaffold durability and functionality [54-56].

XRD patterns confirmed the monoclinic phase of CuO NPs (JCPDS 48-1548), with prominent peaks at 32.75°, 35.70°, and 38.05° 2θ. The absence of Cu_2O peaks indicates high purity. Scherrer's analysis estimated crystallite sizes between 20–50 nm, consistent with SEM observations. The nanoscaffolds exhibited broader peaks (21.35°, 22.97° 2θ), reflecting their semi-crystalline nature, while retained CuO peaks (35.70°, 57.28° 2θ) confirmed NP incorporation. The reduced intensity (~15.9%) and increased peak broadening suggest partial amorphization due to polymer interactions, which may enhance NP dispersion and scaffold flexibility [57-61].

SEM images revealed spherical to irregular CuO NPs (50–200 nm) with some aggregation (500–1000 nm), likely due to surface charge limitations. The starch/PVA nanoscaffolds displayed uniform, bead-free fibers (150–300 nm diameter) with a porous structure, ideal for biomedical applications. Bright protrusions on fiber surfaces confirmed well-dispersed CuO NPs, ensuring effective antimicrobial functionality without compromising scaffold integrity [62, 63].

TGA demonstrated a three-stage degradation profile for CuO-loaded scaffolds, with a residual mass of 64.13%, aligning with expected CuO content (30–40%). The enhanced thermal stability (degradation onset at 262.78°C vs. <250°C for pure starch/PVA) suggests that CuO NPs restrict polymer chain mobility, improving scaffold suitability for high-temperature applications like sterilization [64, 65].

DLS revealed moderate polydispersity (PI: 0.475) with a dominant particle size of 881.5 nm, indicating some aggregation. The zeta potential (-10.03 mV) suggests limited colloidal stability, falling below the ±30 mV threshold for long-term dispersion. Surface modifications (e.g., polymer coatings) could enhance stability for biomedical use [66-70].

The antimicrobial assays demonstrated dose-dependent activity, with nanoscaffolds exhibiting the highest inhibition (e.g., 30±0.16 mm for E. coli), followed by CuO NPs (23±0.58 mm) and algal extract (16±0.83 mm). Similar trends were observed for other pathogens, suggesting synergistic effects between CuO NPs and the polymeric matrix. While ciprofloxacin and voriconazole showed superior activity (26–33 mm), the nanoscaffolds' performance highlights their potential as alternative antimicrobial materials, particularly for wound dressings or coatings [71-73].

The integrated characterization confirms successful CuO NP synthesis, effective embedding into starch/PVA scaffolds, and notable antimicrobial activity. Future work should focus on optimizing NP dispersion and scaffold stability for clinical applications.

5. CONCLUSION

This study successfully demonstrated the green synthesis of CuO NPs using P. variegata extract and their effective incorporation into starch/PVA electrospun nanoscaffolds for antimicrobial applications. Spectroscopic analyses (UV-Vis, FTIR, XRD) confirmed the formation of pure, monoclinic CuO NPs with bioactive phytochemical capping, while SEM revealed uniform nanofiber scaffolds with well-dispersed NPs. The nanoscaffolds exhibited enhanced thermal stability (TGA) and moderate colloidal stability (DLS), though further surface modifications could improve dispersion. Antimicrobial assays highlighted the superior efficacy of CuO-loaded scaffolds against bacterial (E. coli, S. aureus) and fungal (A. niger, Penicillium) pathogens, with inhibition zones comparable to or exceeding those of standalone CuO NPs and algal extract. The synergistic effects of CuO NPs and the polymeric matrix suggest promising potential for biomedical uses, such as wound dressings or antibacterial coatings. Future research should optimize NP loading and scaffold stability for clinical scalability, ensuring prolonged antimicrobial activity and biocompatibility. Overall, this work provides a sustainable, nanocomposite-based strategy to combat microbial resistance.

Ethical Declaration: Not applicable for this study.

Funding: Not available for this study.

Conflicts of Interest: The authors declare no conflicts of interest.

Data Availability Statement: The full dataset of physiochemical characterization associated with this work is published in Mendeley Data [Dataset] Physiochemical characterization of fabricated starch-based nanoscaffolds incorporated with Pocockiella variegata extract-mediated green synthesised copper oxide nanoparticles (DOI: 10.17632/6tddv74p8k.1). Disclosure: The material characterization data and figures (e.g., UV, SEM, FTIR, XRD, TGA, Zeta Potential and particle sizer) presented here were generated from a common dataset and are being reused across multiple related studies on nanomaterials. All biological analyses and conclusions are original to each manuscript.

Disclosure: The material characterization data and figures (e.g., UV, SEM, FTIR, XRD, TGA, Zeta Potential and particle sizer) presented here were generated from a common dataset and are being reused across multiple related studies on nanomaterials. All biological and environmental analyses and conclusions are original to each manuscript.

REFERENCES

1. Umapathy VR, Natarajan PM, Swamikannu B. Regenerative Strategies in Dentistry: Harnessing Stem Cells, Biomaterials and Bioactive Materials for Tissue Repair. Biomolecules. 2025; 15: 546.
2. Ganesan A, Kumar NG, Natarajan PM. Solanum trilobatum leaf extract-derived silver nanoparticles downregulate the PI3K/AKT/mTOR signaling pathway and attenuate oral squamous cell carcinoma cell proliferation. Journal of Herbmed Pharmacology. 2024; 13(2): 300-307.
3. Natarajan PM. Dental Bioinformnatics-Current Scope and Future perspectives. Research Journal of Pharmacy and Technology. 2022;15(5):2351-6.
4. Natarajan PM, Umapathy VR, Murali A, Swamikannu B. (2022). Computational Simulations of Identified marine-derived Natural Bioactive Compounds As Potential Inhibitors of Oral Cancer. Future Science OA. 2022; 8(3).
5. Raju M, Chandrasekaran MK, Loganathan L, Ahalliya RM, Mironescu M, Mironescu ID, Palanisamy CP, Kanniappan GV. Lipid remodeling and ferroptosis in phosphatidylcholine-mediated tumor–stroma crosstalk. Frontiers in Molecular Biosciences. 2026; 13: 1742305.
6. Kunamalla R, Panagal M, Palanisamy CP. Biogenic synthesis and fabrication of starch/PVA/CuO electrospun nanoscaffolds from Sargassum ilicifolium (brown marine macroalgae) extract for anticancer activity on HT-29 and MCF-7 cancer cells. Biocatalysis and Agricultural Biotechnology. 2026; 72: 103923.
7. Pei J, Govindaraj H, Sivaramakrishnan R, Kanniappan GV, Pandurangan V, Dhayalan VK, Mironescu M, Mironescu ID, Jayaraman S, Palanisamy PC. Sustainable fabrication of biopolymer-based (starch/PVA) nanoscaffolds loaded with green-synthesized CuO nanoparticles from Sargassum wightii (marine macroalgae): Cytocompatibility and antioxidant activity. Biomaterials Advances. 2026; 182: 214660.
8. Pei J, Perumal NC, Meng P, Long Q, Palanisamy CP. Extracellular vesicle-based biosensors for Alzheimer's disease: A new frontier in precision diagnostics. Ageing Research Reviews. 2026; 113: 102904.
9. Shree P, Sivaramakrishnan R, Kanniappan GV, Pandurangan V, Jayaraman S, Dhayalan VK, Mironescu M, Mironescu ID, Palanisamy CP. Antioxidant and biocompatible CuO-starch/PVA nanoscaffolds via ultrasonic green synthesis using Turbinaria conoides (brown marine macroalgae). Medicine in Drug Discovery. 2025; 28: 100238.
10. Natarajan PM, Umapathy VR. Role of transcriptomics in the study of oral cancer. Frontiers in Oral Health. 2025; 6:1524364.
11. Natarajan PM, Swamikannu B, Sivaraman NM, Stylin AGSQ. Prevention of Oral Cancer: A Comprehensive Guide. Journal of Pharmacy and Bioallied Sciences. 2024; 16(5): S4239-S4241.
12. Vidhyarekha U, Natarajan PM, Bhuminathan S, Sabarinathan J, Suba R, Vijayalakshmi P. Role of artificial intelligence in Oral Cancer. Advances in Public Health. 2024. 2024: 3664408.
13. Ganesan A, Kumar NG, Natarajan PM, Gauthaman J. Automated classification of elongated styloid processes using deep learning models-an artificial intelligence diagnostics. Frontiers in Oral Health. 2025; 5: 1424840.
14. Gong J, Lin J, Guan T, Pei J, Palanisamy CP, El-AtyFrom AMA. selenium tolerance to nanoplastic antagonism: Comprehensive characterization of L. casei SNUT1 and its extracellular vesicle–nanoselenium complex. Food Bioscience. 2025; 74: 107749.

15. Poochi SP, Sundarraj R, Raju MV, Chandrasekaran MK, Ahalliya RM, Palanisamy CP, Kanniappan GV, Kondapavuluri BK, Thiruvengadam M. Harnessing Nature: Computational and Experimental Insights Into Ipomoea obscura Metabolites for Bladder Cancer Therapy. Chemistry and Biodiversity. 2025; 0: e00909.
16. Dugganaboyana GK, Kannankumar MKG, Shivaramakrishna S, Raju MV, Chandrasekaran MK, Ahalliya RM, Panneerselvam N, Palanisamy CP, Kanniappan GV. Phytochemical insights, antioxidant activity and therapeutic potential of Cassia senna against prostate cancer in Wistar albino rats. Discover Applied Sciences. 2025; 7:1206.
17. Natarajan SR, Krishnamoorthy R, Alshuniaber MA, Gatasheh MK, Rajagopal P, Veeraraghavan VP, Palanisamy CP, Jayaraman S. KDM1A Facilitates Oncogenic Potential in Colorectal Cancer Progression Through the Activation of AXIN/GSK3β/β-Catenin Signaling Pathways: Evidence From Integrated Transcriptomics and In Vitro Studies. The Journal of Gene Medicine. 2025; 27(11): e70053.
18. Guan T, Gong J, Lin J, Palanisamy CP, Jinjin Pei J, El-Aty AMA. Machine learning-driven multimodal optimization of selenium biotransformation and flavor profiling in fermented apple–Yacon functional beverages. Innovative Food Science & Emerging Technologies. 2025; 105: 104198.
19. Natarajan SR, Krishnamoorthy R, Alshuniaber MA, Alsulami TS, Gatasheh MK, Rajagopal P, Palanisamy CP, Govindan R, Veeraraghavan VP, Jayaraman S. ABCE1 facilitates tumour progression via aerobic glycolysis and inhibits cell death in human colorectal cancer cells through the p53 signalling pathway. Scientific Reports. 2025; 15: 24674.
20. Huang Y, Guo H, Liu Y, Jin W, Palanisamy CP, Pei J, Oz F, El-Aty AMA. Effects of Natural Polysaccharides on the Gut Microbiota Related to Human Metabolic Health. Molecular Nutrition & Food Research. 2025; 69:e202400792.
21. Poornima K, Meenakshi K.C, Manikandan V.R, Shankari G, Prabhu D, Rathi M.A, Palanisamy CP, Balaji R, Gopalakrishnan V.K. Exploring the anticancer potential of Jerantinine A from Tabernaemontana coronaria against prostate, breast, and ovarian cancers: A computational approach. Journal of Complementary and Integrative Medicine, 2025 22(2): 363–372.
22. Palanisamy CP, Poompradub S, Sansanaphongpricha K, Jayaraman S, Subramani K. Faridah Sonsudin gGreen synthesis of Nigella sativa-mediated silver nanoparticles for enhanced antibacterial activity and wound healing: Mechanistic insights and biomedical applications. Environmental Nanotechnology, Monitoring & Management. 2025; 24: 101085.
23. Natarajan PM, Bhuminathan S, Leela B, Bindu K, Loganathan K, Ramachandran V. Smoking and its Role in Oral Cancer. Journal of Pharmacy and Bioallied Sciences 16(5): S4242-S4244.
24. Perumal MKK, Renuka RR, Subbiah SK, Natarajan PM. Artificial intelligence-driven clinical decision support systems for early detection and precision therapy in oral cancer: a mini review. Frontiers in Oral Health. 2025; 6: 1592428.
25. Ramesh E, Ganesan A, Lakshmi KC, Natarajan PM. Artificial intelligence-based diagnosis of oral leukoplakia using deep convolutional neural networks Xception and MobileNet-v2. Frontiers in Oral Health. 2025; 6: 1414524.
26. Natarajan PM. Computational Studies on Recent Congeners of Fluoroquinolones and Nitroimidazoles for Their Use in Periodontal Therapy. Journal of Pharmacy and Bioallied Sciences. 2024; 16(5): S4731-S4740.
27. Natarajan PM, Bhuminathan S, Rajan R, Bindu K, Loganathan K, Veerakumar R. The Crucial Role of Smoking Cessation in Preventing Oral Cancer. Journal of Pharmacy and Bioallied Sciences. 2024; 16(5): S4245-S4247.
28. Surendran N, Chandrasekaran G, Raju MV, Chandrasekaran MK, Ahalliya RM, Palanisamy CP, Kanniappan GV, Arcot R, Alharbi NS, Thiruvengadam M. Anti-inflammatory potential of ethanolic extract of Maranta arundinacea L.: Insights from COX-2 modulation and oxidative stress analysis. South African Journal of Botany. 2026; 195: 142-151.
29. Pei J, Senthilkumar MV, Hessini K, Subramaniyam S, Sivaramakrishnan R, Kanniappan GV, Jayaraman S, Palanisamy CP. Green fabrication of starch/PVA/CuO nanoscaffolds using marine macroalgae extract for enhanced anti-inflammatory activity. Sustainable Chemistry and Pharmacy. 2026; 51: 102397.
30. Balasubramanian V, Loganathan L, Muthuswamy K, Viswanathan TM, Raju MV, Chandrasekaran MK, Ahalliya RM, Poorasamy J, Palanisamy CP, Dominic S, Kanniappan GV. Anticancer therapeutic efficacy of PEGylated β-galactosidase from Aspergillus terreus in DMBA-induced breast cancer: Toxicological, molecular and histopathological evaluation in Wistar rats. International Journal of Biological Macromolecules. 2026; 360: 151856.
31. Jayaraman S, Eswaran A, Rajagopal P, Palanisamy CP, Veerakumar P, Veeraraghavan VP, Sirasanagandla SR. Neuroendocrine-associated epigenetic factors in cellular senescence: mechanisms and therapeutic implications. Biogerontology. 2026; 27(2): 64.
32. Ponnusamy B, Rajagopal P, Palanisamy CP, Veeraraghavan VP, Jayaraman S. Mechanistic Exploration of the anticancer activity of Justicia adhatoda Plant Leaf Ethanolic Extract against Colon Cancer Cells: An in silico and in vitro Approach. Asian Pacific Journal of Cancer Prevention. 2026; 27(3): 1069-1080.
33. Pei J, Saran VS, Sivaramakrishnan R, Kanniappan GV, Pandurangan V, Jayaraman S, Dhayalan VK, Mironescu M, Mironescu ID, Palanisamy CP. Ultrasonic-assisted, Sargassum ilicifolium (brown marine macroalgae)-mediated biogenic synthesis of CuO nanoparticles incorporated in starch/PVA electrospun nanoscaffolds: In vitro safety and antioxidant efficacy assessment. Bioorganic Chemistry. 2026; 173: 109679.
34. Raj MAPA, Subramaniyam S, Kanniappan GV, Jayaraman S, Palanisamy CP. Sustainable fabrication of starch/PVA/CuO electrospun nanoscaffolds from Turbinaria ornata (marine macroalgae) extract: Physicochemical characterization and antidiabetic evaluation. Kuwait Journal of Science. 2026; 53(2): 100545.
35. Pei J, Ganesh NS, Subramaniyam S, Sivaramakrishnan R, Kanniappan GV, Jayaraman S, Palanisamy CP. Sustainable fabrication of starch/PVA/CuO electrospun nanoscaffolds from Padina tetrastromatica (Brown macroalgae) extract: Physicochemical characterization and antidiabetic assessment. Sustainable Chemistry One World. 2026; 9: 100195.
36. Sakthiraj A, Sivaramakrishnan R, Subramaniyam S, Kanniappan GV, Pandurangan V, Jayaraman S, Dhayalan VK, Mironescu M, Mironescu ID, Palanisamy CP. Chemical Physics Impact. Starch/PVA electrospun nanoscaffolds loaded

with ultrasonic-assisted green-synthesis of CuO nanoparticles from marine macroalgae (Gracilaria corticata) extract: Cytotoxicity and antioxidant analysis. 2026; 12: 101018.
37. Ganesan A, Kumar NG, Natarajan PM. Anticancer activity of silver nanoparticles synthesized from aqueous leaf extract of Solanum trilobatum (Purple fruit pea eggplant) on human oral cancer cells. Journal of Herbmed Pharmacololgy. 2024; 13(2): 260-268.
38. Umapathy V, Dhanavel A, Kesavan R, Natarajan PM, Bhuminathan S, Vijayalakshmi P. Anticancer Potential of the Principal Constituent of Piper nigrum, Piperine: A Comprehensive Review. Cureus. 2024; 16(2): e54425.
39. Umapathy VR, Swamikannu B, Natarajan PM, Devi R, Nandini MS, Vimalarani, Vijayalakshmi P. In Silico Molecular Docking of Ocimum sanctum Phytochemicals: Targeting Key Biomarkers in Oral Cancer. Journal of Pharmacy and Bioallied Sciences. 2024; 16(5): S4792-S4799.
40. Swamikannu B, Umapathy VR, Natarajan PM, Nandini MS, Stylin AGSQ, Vimalarani V, Rajinikanth S. Unlocking the Therapeutic Benefits of Artemisia Annua: A Comprehensive Overview of its Medicinal Properties. Journal of Pharmacy and Bioallied Sciences. 2024; 16(5): S4248-S4253.
41. Yadalam PK, Arumuganainar D, Natarajan PM, Ardila CM. Artificial intelligence-powered prediction of AIM-2 inflammasome sequences using transformers and graph attention networks in periodontal inflammation. Scientific Reports. 2025; 15: 8733.
42. Yadalam PK, Chatterjee S, Natarajan PM, Ardila CM. Comparison of light gradient boosting and logistic regression for interactomic hub genes in Porphyromonas gingivalis and Fusobacterium nucleatum-induced periodontitis with Alzheimer's disease. Frontiers in Oral Health. 2025; 6:1463458.
43. Yadalam PK, Natarajan PM, Ardila CM. Variational graph autoencoder for reconstructed transcriptomic data associated with NLRP3 mediated pyroptosis in periodontitis. Scientific Reports. 2025; 15: 1962.
44. Surendran N, Raju MV, Chandrasekaran MK, Ahalliya RM, Palanisamy CP, Chandrasekaran G, Kanniappan GV. Physicochemical characterization of starch from Maranta arundinacea L.(arrowroot) rhizomes and its inhibition of COX-2: In vivo validation. Bioactive Carbohydrates and Dietary Fibre. 2025; 33: 100465.
45. Kannappan P, Chandrasekaran MK, Raju MV, Gopalakrishnan S, Dhamodharan P, Ahalliya RM, Palanisamy CP, Raju B, Kanniappan GV. Exploring the anticancer potential of Jerantinine A from Tabernaemontana coronaria against prostate, breast, and ovarian cancers: a computational approach. Journal of Complementary and Integrative Medicine. 2025; 22(02): 363-372.
46. Pei J, Kumarasamy RV, Jayaraman S, Kanniappan GV, Long Q, Palanisamy CP. Quercetin-functionalized nanomaterials: Innovative therapeutic avenues for Alzheimer's disease management. Ageing Research Reviews. 2025; 104: 102665.
47. Jayaraman S, Prasad M, Natarajan SR, Krishnamoorthy R, Alshuniaber MA, Gatasheh MK, Veeraraghavan VP, Rajagopal P, Palanisamy CP. Molecular mechanisms underlying the effects of beta-sitosterol on TGF-β1/Nrf2/SIRT1/p53-mediated signaling in the kidney of a high-fat diet and sucrose-induced type-2 diabetic rat. Chemico-Biological Interactions. 2025; 411: 111443.
48. Huang Y, Guo H, Liu Y, Jin W, Palanisamy CP, Pei J, Oz F, El-Aty AMA. Effects of Natural Polysaccharides on the Gut Microbiota Related to Human Metabolic Health. Molecular Nutrition & Food Research. 2025; e202400792.
49. Prabhakaran P, Palanisamy CP, Shanmugam A, Damodharan P, Swaminathan H, Devaraj D, Ahalliya RM, Kanniappan GV. Isolation, structural characterization, and molecular docking studies on the bioactive compound from n-Hexane extract of Emilia sonchifolia (L.) DC against the pancreatic cancer target Aurora 2 Kinase. Journal of Complementary and Integrative Medicine. 2024; 22(1): 0290.
50. Jiang H, Kumarasamy RV, Pei J, Raju K, Kanniappan GV, Palanisamy CP. Integrating engineered nanomaterials with extracellular vesicles: Advancing targeted drug delivery and biomedical applications. Frontiers in Nanotechnology. 2024; 6: 1513683.
51. Guo H, Liu Y, Wan T, Song D, Palanisamy CP, Geng J, Pei J, Özmen S, El-Aty AMA. Toward personalized cancer management: Role of precision nutrition–diet interventions. Journal of Functional Foods. 2024; 123: 106584.
52. Natarajan SR, Krishnamoorthy R, Alshuniaber MA, Al-Anazi KM, Farah MA, Rajagopal P, Palanisamy CP, Veeraraghavan VP, Jayaraman S. Identification of FOXM1 as a novel protein biomarker and therapeutic target for colorectal cancer progression: Evidence from immune infiltration and bioinformatic analyses. International Journal of Biological Macromolecules. 282 (Part 4): 137201.
53. Rajendran MS, Jayaraman S, Khan JM, Jasmine S, Prabhakaran RK, Raju MV, Chandrasekaran MK, Ahalliya RM, Kannappan P, Palanisamy CP, Kanniappan GV. Investigating the colon toxicity and carcinogenic role of monosodium glutamate compared with Dimethylhydrazine in male Wistar rats: Exploring the link to childhood colon cancer risk. Journal of King Saud University - Science. 2024; 36(11): 103507.
54. Kumarasamy RV, Natarajan PM, Umapathy VR, Roy JR, Rab SO, Saeed M, Panagal M, Mironescu M, Srinivasan GP, Palanisamy CP. Clinical Applications and Therapeutic Potentials of Advanced Nanoparticles: A Comprehensive Review on Completed Human Clinical Trials. Frontiers in Nanotechnology. 2024; 6:1479993.
55. Jin W, Pei JJ, Roy JR, Jayaraman S, Ahalliya RM, Kanniappan GV, Mironescu M, Palanisamy CP. Comprehensive review on single-cell RNA sequencing: A new frontier in Alzheimer's disease research. Ageing Research Reviews. 2024; 274: 102454.
56. Pei J, Palanisamy CP, Jayaraman S, Natarajan PM, Umapathy VR, Roy JR, Panagal M, Jayaraman S. Curcumin-loaded polymeric nanomaterials as a novel therapeutic strategy for Alzheimer's disease: A comprehensive review. Ageing Research Reviews. 2024; 99: 102393.

57. Pei J, Palanisamy CP, Jayaraman S, Natarajan PM, Umapathy VR, Roy JR, Thalamati D, Ahalliya RM, Kanniappan GV*, Mironescu M. A comprehensive review on starch-based Sustainable Edible Films Loaded with Bioactive Components for Food Packaging. International Journal of Biological macromolecules. 2024; 274 (Part-1): 133332.
58. Palanisamy CP, poompradub S, Sansanaphongpricha K, Subramani K, Sonsudin F. Increased expression levels of PDGF and VEGF magnify the wound healing potential facilitated by biogenic synthesis of silver nanoparticles. Nano-Structures & Nano-Objects. 2024; 39: 101236.
59. Pei J, Palanisamy CP, Jayaraman S, Natarajan PM, Umapathy VR, Roy JR, Thalamati D, Ahalliya RM, Kanniappan GV, Mironescu M. Proteomics Profiling of Extracellular Vesicle for Identification of Potential Biomarkers in Alzheimer's Disease: A Comprehensive Review. Ageing Research Reviews. 2024; 99: 102359.
60. Xi J, Wang T, Xian P, Liu X, Du M, Yang H, Palanisamy CP, Lin W, Long Q. Proteomic insights uncover enhanced neurotherapeutic potential in conditioned mesenchymal stem cell-derived extracellular vesicles. Extracellular Vesicle. 2024; 3: 100037.
61. Pei J, Natarajan PM, Umapathy VR, Swamikannu B, Sivaraman NM, Krishnasamy L, Palanisamy CP. Advancements in the synthesis and functionalization of zinc oxide-based nanomaterials for enhanced oral cancer therapy. Molecules. 2024; 29(11): 2706.
62. Gatasheh MK, Natarajan SR, Krishnamoorthy R, Alsulami TS, Rajagopal P, Palanisamy CP, Veeraraghavan VP, Jayaraman S. Molecular analysis to identify novel potential biomarkers as drug targets in colorectal cancer therapy: an integrated bioinformatics analysis. Molecular and Cellular Oncology. 2024; 11(1): 2326699.
63. Pei J, Yan Y, Jayaraman S, Rajagopal P, Natarajan PM, Umapathy VR, Gopathy S, Roy JR, Sadagopan CS, Thalamati D, Palanisamy CP, Mironescu M. A review on advancements in the application of starch-based nanomaterials in biomedicine: Precision drug delivery and cancer therapy. International Journal of Biological Macromolecules. 2024; 130746.
64. Pei JJ, Yan Y, Palanisamy CP, Jayaraman S, Natarajan PM, Umapathy VR, Gopathy S, Roy JR, Sadagopan JC, Thalamati D, Mironescu M. Materials-based drug delivery approaches: Recent advances and future perspectives. Green Processing and Synthesis. 2024; 13: 20230094.
65. Panneerselvam S, Viswaja K, Deepa E, Prathiba S, Rebecca FS, Nivedha RP, Rajagopal P, Veeraraghavan VP, Sridevi G, Palanisamy CP, Jayaraman S. Hypoglycemic Potential of Acalypha indica in Streptozotocin-Induced Type 2 Diabetic Rats. International Journal of Drug Delivery Technology. 2026; 16(26s):1038-1047.
66. Panneerselvam S, Viswaja K, Prathiba S, Rebecca FS, Nivedha RP, Rajagopal P, Fathima SJH, Veeraraghavan VP, Sridevi G, Palanisamy CP, Jayaraman S. Acalypha Indica Attenuates Insulin Resistance in STZ-Induced Type 2 Diabetic Male Rats: Mechanistic Study. International Journal of Drug Delivery Technology. 2026; 16(26s):1027-1037.
67. Manju NE, Natarajan A, Rebecca FS, Nivedha RP, Hemalatha R, Rajagopal P, Murali R, Veeraraghavan VP, Sridevi G, Palanisamy CP, Jayaraman S. Effect of Seendhil polyherbal formulation in attenuating type-2 diabetes in STZ-induced experimental rats. International Journal of Drug Delivery Technology. 2026; 16(26s):981-989.
68. Manju NE, Natarajan A, Rebecca FS, Nivedha RP, Hemalatha R, Rajagopal P, Murali R, Veeraraghavan VP, Sridevi G, Palanisamy CP, Jayaraman S. Molecular mechanism to identify the effects of Seendhil polyherbal preparation on IRS-1/AKT/GLUT4/NRF2-KEAP-1 mediated signaling in SFZ-induced type-2 diabetic adult male rats. International Journal of Drug Delivery Technology. 2026;16(26s):972-980.
69. Palanisamy CP, Poompradub S, Sansanaphongpricha K, Jayaraman S, Subramani K, Sonsudin F. Biosynthesis of silver nanoparticles (AgNPs) using ethanolic extract of Nigella sativa (L.) seeds promotes wound healing via PDGF and VEGF signalling pathways activation. Biocatalysis and Agricultural Biotechnology. 2023; 54: 102970.
70. Palanisamy CP, Pei JJ, Phaniendra A, Venkata AAN, Jayaraman S, Veeraragahavan VP, Sridevi G, Roy JR, Janaki CS, Thalamati D, Mironescu M, Luo Q, Chai Y, Long Q. New Strategy of Neurodegenerative Disease Treatment with Extracellular Vesicles (EVs) Derived from Mesenchymal Stem Cells (MSCs). Theranostics. 2023; 13(12):4138-4165.
71. Hashemi SB, Rahimi A, Arjmand M. Extraction of Nutraceutical Bioactive Compounds from Native Algae Using Solvents with a Deep Natural Eutectic Point and Ultrasonic-Assisted Extraction. Computational Research Progress in Applied Science & Engineering. 2023;9(02):1-12.
72. Anbalagan G, Subramanian B, Suresh V, Sivaperumal P. Green synthesis of copper and copper oxide nanoparticles from brown algae turbinaria species' aqueous extract and its antibacterial properties. Cureus. 2024;16(4).
73. Filimon A, Dobos AM, Onofrei MD, Serbezeanu D. Polyvinyl Alcohol-Based Membranes: A Review of Research Progress on Design and Predictive Modeling of Properties for Targeted Application. Polymers. 2025;17(8):1016.